

Effects of Elastic Modulus on Single Fiber Uniaxial Deformation

Undergraduate Honors Thesis

Presented in Partial Fulfillment of the Requirements for Graduation with Distinction

at The Ohio State University

By

Jacqueline Ohmura

The Ohio State University

2011

Defense Committee:

Dr. Peter Anderson, Adviser

Dr. Heather Powell

ABSTRACT

Tissue engineering offers reductions in both mortality and morbidity of tissue recipients as well as the possibility of a vast pool of implantable tissues. Regrettably, use of engineered tissue is limited by mechanical properties that are insufficient compared to native tissues. A promising avenue to improve this deficiency is mechanical stimulation. Mechanical stimulation, such as the introduction of a cyclical load during tissue formation, is a multi-step process beginning with the translation of scaffold material properties into scaffold micro-deformation. The present study explored this relationship by characterizing the effect of scaffold elastic modulus and initial fiber geometry on scaffold micro-deformation. Finite element modeling was utilized to simulate three geometrically identical sets of 100 unique fiber shapes, with differing elastic moduli of 10 MPa, 100 MPa, and 1000 MPa. Fibers were then strained to 20% strain via ABAQUS, finite element software. Normalized force curves during the straining process, as well as fiber geometry characterized via sine Fourier series and tortuosity, were calculated for each fiber set at 0 and 20% strain. Single fiber deformation appeared to be independent of fiber modulus. This study also indicated that amplitudes of fiber Fourier coefficients reduce proportionally during uniaxial extension, revealing a $75\pm 7\%$ reduction in wavelength amplitude from 0 to 20% strain in all fiber sets. By further defining the role of scaffold mechanics in mechanical stimulation, it is projected that this research will provide a platform for rapid optimization of external environment for tissue growth.

ACKNOWLEDGMENTS

I would like to thank my advisors Dr. Peter Anderson and Dr. Heather Powell, as well as Greg Ebersole for all of their assistance, support, and guidance with all aspects of this thesis.

TABLE OF CONTENTS

CHAPTER 1: INTRODUCTION	- 1 -
1.1 Introduction: The necessity for tissue engineering	- 1 -
1.2 Motivation: Improvement of engineered tissue mechanical properties through mechanical stimulation.....	- 2 -
1.3 Literature Review: Traditional methods of describing scaffold geometry and micro- scale deformation	- 4 -
1.4 Project Objective.....	- 4 -
CHAPTER 2: METHOD AND MODELS	- 6 -
2.1 Finite element modeling of Fiber Sets	- 6 -
2.1.1 Scaffold Fabrication and Imaging.....	- 6 -
2.1.2 Determining in vitro fiber geometries	- 6 -
2.1.3 Finite element model creation.....	- 8 -
2.2 Strain simulation	- 9 -
2.3 Geometric analysis of strained and unstrained fibers	- 10 -
2.5.1 Fourier coefficients	- 10 -
2.5.2 Tortuosity	- 12 -
2.4 Post-processing analysis	- 12 -
CHAPTER 3: RESULTS	- 14 -
3.1 Stress-strain behavior of single fibers.....	- 14 -
3.2 Geometric changes in single fibers from 0 to 20% strain	- 15 -
3.2.1 Fourier coefficient changes.....	- 15 -
3.2.2 Tortuosity changes.....	- 18 -
CHAPTER 4: DISCUSSION	- 20 -
4.1 Stress-strain behavior of single fibers in uniaxial deformation	- 20 -

4.1.1	Toutuosity dependence	- 20 -
4.1.2	Stiffness independence.....	- 21 -
4.2	Single fiber geometry changes between strained and unstrained conditions	- 22 -
4.2.1	Independence of average geometry changes with respect to fiber elastic modulus - 22 -	
4.2.2	Proportional reduction in Fourier amplitudes during straining.....	- 22 -
4.2.3	Proposed relationships between individual fiber stiffness and fiber geometry changes <i>in vitro</i> fiber extension.....	- 23 -
CHAPTER 5: CONCLUSIONS AND FUTURE WORK		- 25 -
5.1	Conclusions	- 25 -
5.2	Future work.....	- 25 -
BIBLIOGRAPHY.....		- 27 -
APPENDIX A		- 29 -
APPENDIX B		- 32 -

LIST OF FIGURES

Figure 1: Donors and wait list values for the past 10 years [5]	2 -
Figure 2: Change progression occurring in engineered tissues during mechanical stimulation .-	3 -
Figure 3: Example of ImageJ x,y coordinate measurements	7 -
Figure 4: Pictorial representation of 3 fiber sets E is in MPa.....	8 -
Figure 5: Two separate fibers of distinct geometries from the 10MPa set before strain A & C and after strain, B & D.	9 -
Figure 6: Process used to prepare strained fiber data for DFT. A) Depicts the final strained fiber shape with coordinates from x=0 to x=240; B) depicts the interpolated fiber shape from x=0 to x=200; C) depicts the fiber reorientation process.	11 -
Figure 7: Comparison of normalized stress versus strain of fibers listed in Table 3.	14 -
Figure 8: Average amplitudes of Fourier coefficients for fibers in the non strained condition (red), as well as fibers of 10 (green), 100 (blue), and 1000MPa (purple) at the 20% condition. -	15 -
Figure 9: Average percent decrease in amplitude from unstrained to 20% strained geometry for each Fourier coefficient. Data is presented for fibers with E=10MPa (green), E=100MPa (blue), and E=1000MPa (purple)	16 -
Figure 10: Average amplitudes of Fourier coefficients for fibers in the non strained condition, as well as fibers of 10, 100, and 1000MPa at the 20% condition	19 -

LIST OF TABLES

Table 1: Performed matched pair t-tests.....	- 13 -
Table 2:Attributes of fibers plotted in Figure 8. Along with distinct Fourier coeffieicnts, configuration 'a' corresponds with an initial tortuosity of while configuration 'b' corresponds with an initial tortuosity	- 15 -
Table 3: Average amplitudes of Fourier coefficients for fibers in the non strained condition, as well as fibers of 10, 100, and 1000MPa at the 20% condition	- 17 -
Table 4: Matched pair t-test results for the comparison of average tortuosity values in the 20% strain fiber sets	- 19 -

CHAPTER 1: INTRODUCTION

This chapter provides an introduction to the topic of tissue engineering with particular emphasis on the necessity to optimize mechanical stimulation. Section 1.1 describes the current status of tissue and organ replacement techniques, while section 1.2 provides motivations behind this study. Section 1.3 includes a literature review of relevant topics. Finally, section 1.4 discusses the project objective.

1.1 Introduction: The necessity for tissue engineering

While the number of donor tissues and organs has experienced a slight increase over the past ten years, the number of people waiting for these transplants has continued to rise dramatically. Figure 1 illustrates this trend. In addition to availability issues, traditional procedures of tissue grafting and transplants are also limited by cost and complication risks. Complication risks associated with these types of treatments include the potential of disease transmission, risk of immune rejection, as well as morbidity at the donor site [2]. Similarly, the costs associated with transplants and tissue grafts are rooted in multiple factors. The US average for heart-only transplants in 2008, for instance, was \$787,700 due organ recovery fees, additional stays of hospital complications, anti-rejection drugs, and follow up care [3,4].

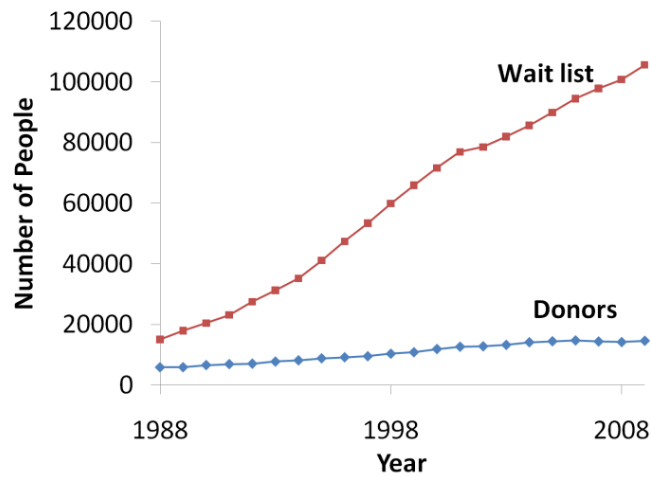


Figure 1: Donors and wait list values for the past 10 years [5]

Fortunately, tissue engineering provides the opportunity to reduce problems of scarcity, certain complications, and costs associated with traditional tissue and organ replacement techniques. With respect to scarcity, tissue engineering offers the potential for an unlimited pool of organs and tissues for implantation. With respect to complications, tissue engineering has exhibited reduction in surgical procedures, morbidity, mortality, and immune system response [1,2,6,7]. And with respect to cost, tissue engineering reduces many sources of expense including immune-suppression treatments, operating time, and frequency of complications requiring additional surgeries [3].

1.2 Motivation: Improvement of engineered tissue mechanical properties through mechanical stimulation

Although tissue engineering offers many benefits to organ culture technology, it is often limited in utilization due to disparity in mechanical properties and biological function of engineered tissues, as compared to their native counterparts. In order to significantly

improve mechanical properties in engineered tissue while maintaining biologic function, mechanical stimulation has been utilized. This process applies typical *in vivo* forces to maturing tissues via mechanical bioreactors increasing macro-scale tissue properties through the multi-step, multi-scale progression depicted in Figure 2.



Figure 2: Change progression occurring in engineered tissues during mechanical stimulation

To date, mechanical stimulation has yielded significant effects on mechanical properties such as strength and stiffness, as well as orientation, cell proliferation, and gene expression [8,9,10]. Although benefits of mechanical stimulation have been documented, currently no model exists to determine the optimal mechanical environment for the growth of tissues. This is partly due to the lack of rigorous characterization of the relationship between macro-scale scaffold properties and micro-scale scaffold deformation, labeled as relationship ‘1’ in Figure 2. As a result, it is the goal of this study to contribute to a large scale model which would assist in determination of optimal mechanical stimulation profiles for engineered tissue by exploring not only micro-scale deformation mechanisms, but also the effect of scaffold elastic modulus on micro-scale scaffold deformation.

1.3 Literature Review: Traditional methods of describing scaffold geometry and micro-scale deformation

In order to analyze scaffold micro-deformation through analyzing changes in fiber geometry, a robust and accurate method of describing scaffold geometry is required. Multiple methods have been developed for the purpose of describing scaffold geometry including: mean intercept length (MIL), line fraction deviation (LFD), and Fourier transform methods (FTM). MIL is performed by analyzing the number of intersections of fibers with a predetermined grid, while LFD is a more sophisticated version of MIL [11]. FTM is based on fitting the coordinates of a fiber into constituent frequencies. It has been indicated, however, that FTM is the most reliable process in characterizing geometry and is more easily adaptable to processes than MIL and LFD [12]. This was confirmed through both simulation as well as experimentation with fibrin gels. As a result, this study utilizes FTM in its characterization of scaffold fiber geometries, for it is not only conducive to single fiber measurements, but is also the more accurate choice for a matrix of fibers which is important for the end goal of adaptability to a multi-fiber model.

1.4 Project Objective

The main objective of this study was to characterize the method of geometric deformation of single fibers of a tissue engineering scaffold with emphasis on the effects of scaffold elastic modulus on deformation geometry. This project focused on two hypotheses :

- 1) Increased scaffold elastic modulus will affect the geometric evolution of a fiber during strain, specifically the rate at which Fourier amplitudes of a fiber decrease with extension in relation to one another.
- 2) During general uniaxial extension in a single fiber, large wavelengths in the fiber geometry will reduce faster with elongation than small wavelength Fourier components in the single fiber.

The knowledge gleaned from this study will inform an *in silico* linking scaffold mechanical and chemical properties to scaffold micro-deformation during mechanical stimulation, and will interface with relationship '1' depicted in Figure 2. Once completed, this model will connect the link between scaffold properties and the origin of cellular signaling, thus providing a platform for the determination of optimal physical and mechanical environments for all engineered tissues.

CHAPTER 2: METHOD AND MODELS

2.1 Finite element modeling of Fiber Sets

2.1.1 Scaffold Fabrication and Imaging

Collagen (SENED S) scaffolds were electrospun using a 10% w/v solution in 1,1,1,3,3,3-hexafluoro-2-propanol (HFP, Sigma, St. Louis, MO). Rhodamine was added to the collagen at a 1% w/v for the purpose of fluorescent imaging. The scaffolds were spun with a working distance of 20 cm and a potential of 30kV in order to produce 0.5 μ m fibers. Scaffolds were cross-linked for 24 hours at 140 °C by vacume dehydration then chemically cross-linked for 24 hours with a 5mM solution of 1-ethyl-3-(3-dimethylaminopropyl)carbodiimide hydrochloride (EDC, Sigma, St. Louis, MO) in 100% EtOH. After fabrication, confocal z-stacks of the scaffolds were taken at a .3 μ m slice size.

2.1.2 Determining in vitro fiber geometries

Geometries of *in vitro* fibers were determined by recording fiber position through sequential x,y, and z coordinates. Collected z-stacks were first subjected to pixel intensity filtration in order to separate fibers onto specific z-planes. Through this

method, fibers with the most intense pixels were assumed to be located on the upper plane of the optical slice. Once identified, these fibers were removed as they did not lie on the plane of interest. For the remaining fibers, a grid was superimposed onto the confocal image via ImageJ software. Then x,y cartesian coordinates were assigned to the fiber spaced in increments of 10μ on the x-axis as illustrated in Figure 3. In this fashion, every visible fiber which extended 200μ within the field of view, the minimum length required for the specific DFT utilized in the geometric analysis described in 2.4.2, was analyzed to avoid bias in fiber selection.

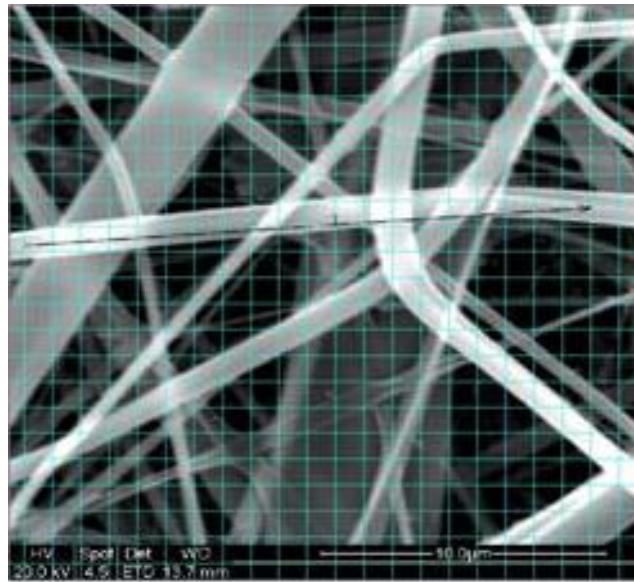


Figure 3: Example of ImageJ x,y coordinate measurements

2.1.3 Finite element model creation

Three sets of 100 fibers were modeled using finite element modeling via ABAQUS. One set of fibers was modeled with $E = 10\text{MPa}$, the second set was modeled with $E = 100\text{MPa}$, while final set was modeled with $E = 1000\text{MPa}$. Geometries of the fibers were based on 100 of the collected *in vitro* collagen geometries. Except for Young's modulus (E), all three fiber sets were modeled to the exact same specifications. In addition to the same fiber geometries, all fibers were given a radius of $.5\text{ }\mu\text{m}$, the average fiber diameter of the collagen fibers, a linear elastic regime, and a projected end to end length of $200\text{ }\mu\text{m}$. A sample input file representative of a single fiber model can be found in Appendix A. Figure 4 depicts a representation of the three fiber sets modeled in ABAQUS.

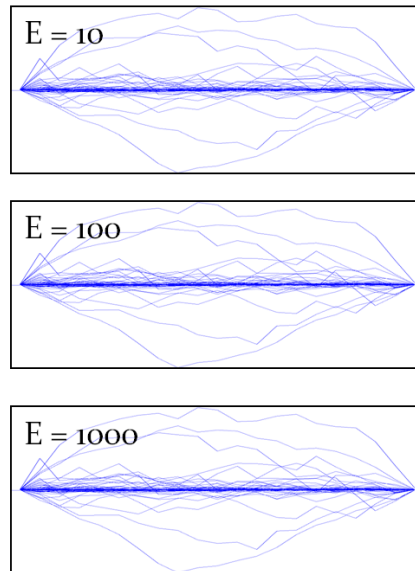


Figure 4: Pictorial representation of 3 fiber sets E is in MPa

2.2 Strain simulation

Fibers were strained to 20% in ABAQUS as depicted in Figure 5. The reaction force exerted on the fibers during strain as well as the coordinates of the fibers at 20% strain were recorded for each fiber for further analysis. Stretching was accomplished by specifying separation of the fiber end points until points were 240um apart from each other, coinciding with 20% nominal extension. Moments were not applied at the end points.

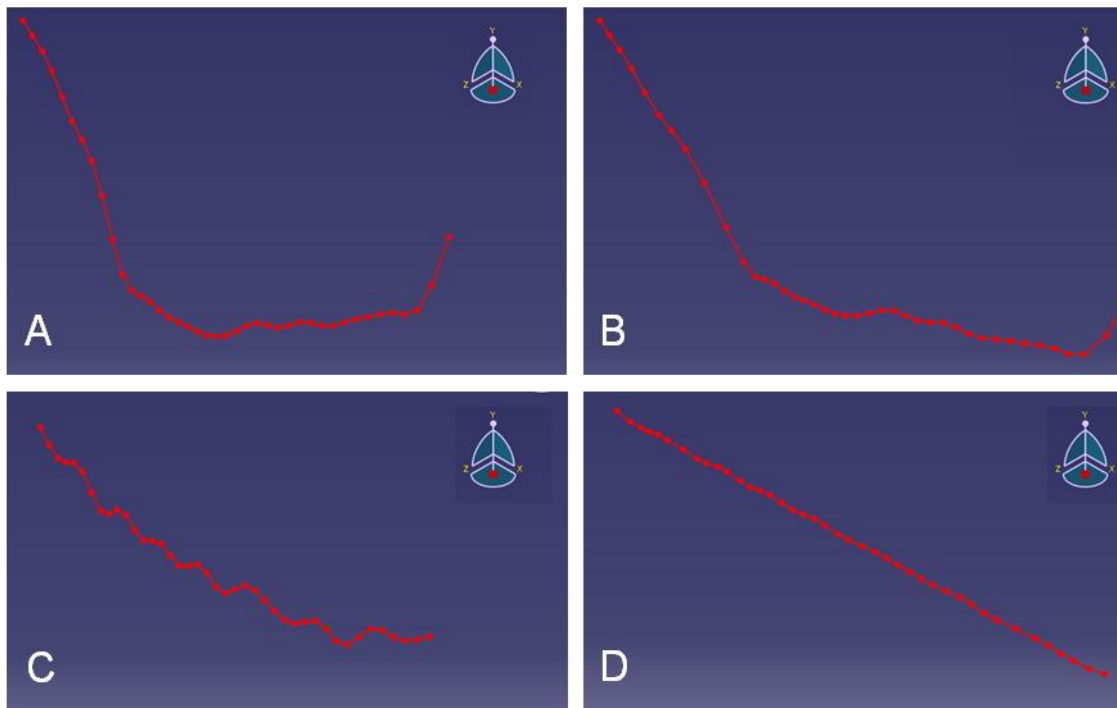


Figure 5: Two separate fibers of distinct geometries from the 10MPa set before strain A & C and after strain, B & D.

2.3 Geometric analysis of strained and unstrained fibers

Cartesian coordinates of the fibers were utilized to determine the discrete Fourier coefficients as well as the tortuosity of each fiber. The following subsections describe the equations and methods utilized in these calculations.

2.5.1 Fourier coefficients

Fourier coefficients were determined with a sine series, and corresponded to the following equations [14],

$$y(x) = \frac{1}{N} \sum_{k=0}^{N-1} a_k \sin \frac{\pi k x}{N}$$

Equation 1

where a_k is the amplitude of each wave is,

$$a_k = 2 \sum_{n=0}^{N-1} y_n \sin \frac{\pi k n}{N}$$

Equation 2

and N is 20.

In order to perform discrete Fourier transform on each fiber in a consistent manner, coefficients were determined using the following process:

1. Final fiber coordinates were obtained from $x=0$ to $x=200 \mu\text{m}$ for all fibers
2. Fibers were re-oriented such the fiber was oriented to the points $(0,0)$ and $(200,0)$, with the start of the fiber coinciding with the coordinates $(0,0)$.

3. Coordinate pairs evaluated for each fiber started at $x=0$ and increased in increments of $\Delta x = 10\mu\text{m}$ along the x-axis

For ease of calculation, the original fiber coordinate pairs *in vitro* were measured in increments of 10 along the x-axis, starting at (0,0) and ending at (200,0). As a result, reorientation and interpolation was not required in order to perform DFT on these fibers. Strained fibers, however, required reorientation of the fiber to run through the points (0,0) and (200,0). Interpolation of coordinate sets was also required to obtain x,y pairs for x values starting at 0 and increasing in increments of 10. Figure 6 illustrates the process used to prepare strained fibers for discrete Fourier transform analysis, while Appendix B contains the code used in this preparation.

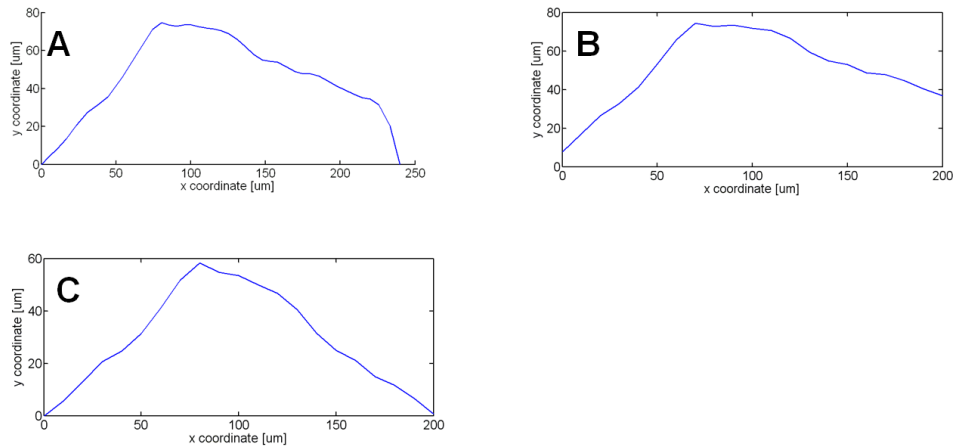


Figure 6: Process used to prepare strained fiber data for DFT. A) Depicts the final strained fiber shape with coordinates from $x=0$ to $x=240$; B) depicts the interpolated fiber shape from $x=0$ to $x=200$; C) depicts the fiber reorientation process.

2.5.2 Tortuosity

Tortuosity was calculated using Equation 3. A piece-wise linear approximation was used to determine overall fiber length.

$$Tortuosity = \frac{Fiberlength}{Fiber_endtoend_length} \quad \text{Equation 3}$$

2.4 Post-processing analysis

Matched pair t-tests were performed on the resulting Fourier coefficients values with a confidence level of 95%. Matched pair t-tests were performed by computing the t-statistic for the set of differences between two populations. The t-tests were performed to determine if the 20% strained Fourier coefficients of the E=10MPa, E=100MPa, and E=1000MPa sets belonged to the same or different populations, thus testing for a significant difference in final Fourier coefficients based on fiber moduli. This process was repeated for each Fourier coefficient, as well as tortosity values comparing the 20% strained E=10MPa, E=100MPa, and E=1000MPa sets to one another.

Table 1: Performed matched pair t-tests

	Compared populations*	
Test 1	E=10 MPa Fiber set	E = 100 Mpa Fiber set
Test 2	E= 10 Mpa Fiber set	E= 1000 Mpa Fiber set
Test 3	E=100MPa Fiber set	E=1000MPa Fiber set

* all values correspond to 20% strain

CHAPTER 3: RESULTS

This chapter reports the results of the study. Section 3.1 discusses the independence of normalized stress-strain curves on fiber modulus. Section 3.2 describes the proportional decrease observed in Fourier coefficients between 0 and 20% strain as well as the independence of the decrease on fiber modulus. Finally, section 3.3 reports the independence of fiber tortuosity changes with respect to fiber modulus.

3.1 Stress-strain behavior of single fibers

Normalized stress-strain curves exhibited two trends observed in the stress-strain behavior of observed fibers. First, the stress-strain behavior of the fibers was found to be independent of fiber modulus. Second, fiber tortuosity dictated the stress-strain behavior of the fiber. Figure 7 depicts these trends, through the depiction of the normalized stress-strain curves of six fibers with the attributes described in Table 2. Fibers 1-3 exhibited the same stress-strain behavior. Similarly, fibers 4-6 exhibited the same stress-strain behavior. Thus, independence of normalized fiber stress-strain response on modulus is indicated. In Figure 7, it can also be seen that the stress-strain behavior of fibers with

‘configuration a’, a more tortuous initial geometry than ‘configuration b’, exhibit a different stress-strain response than fibers of a ‘configuration b’ geometry. Thus,

Figure 7 also depicts the disparity in fiber stress-strain behavior based on fiber tortuosity.

Table 2: Attributes of fibers plotted in Figure 8. Along with distinct Fourier coefficients, configuration ‘a’ corresponds with an initial tortuosity of while configuration ‘b’ corresponds with an initial tortuosity .

	Initial Tortuosity	Geometry	Moduli [MPa]
Single fiber 1	1.5	configuration a	10
Single fiber 2	1.5	configuration a	100
Single fiber 3	1.5	configuration a	1000
Single fiber 4	1.2	configuration b	10
Single fiber 5	1.2	configuration b	100
Single fiber 6	1.2	configuration b	1000

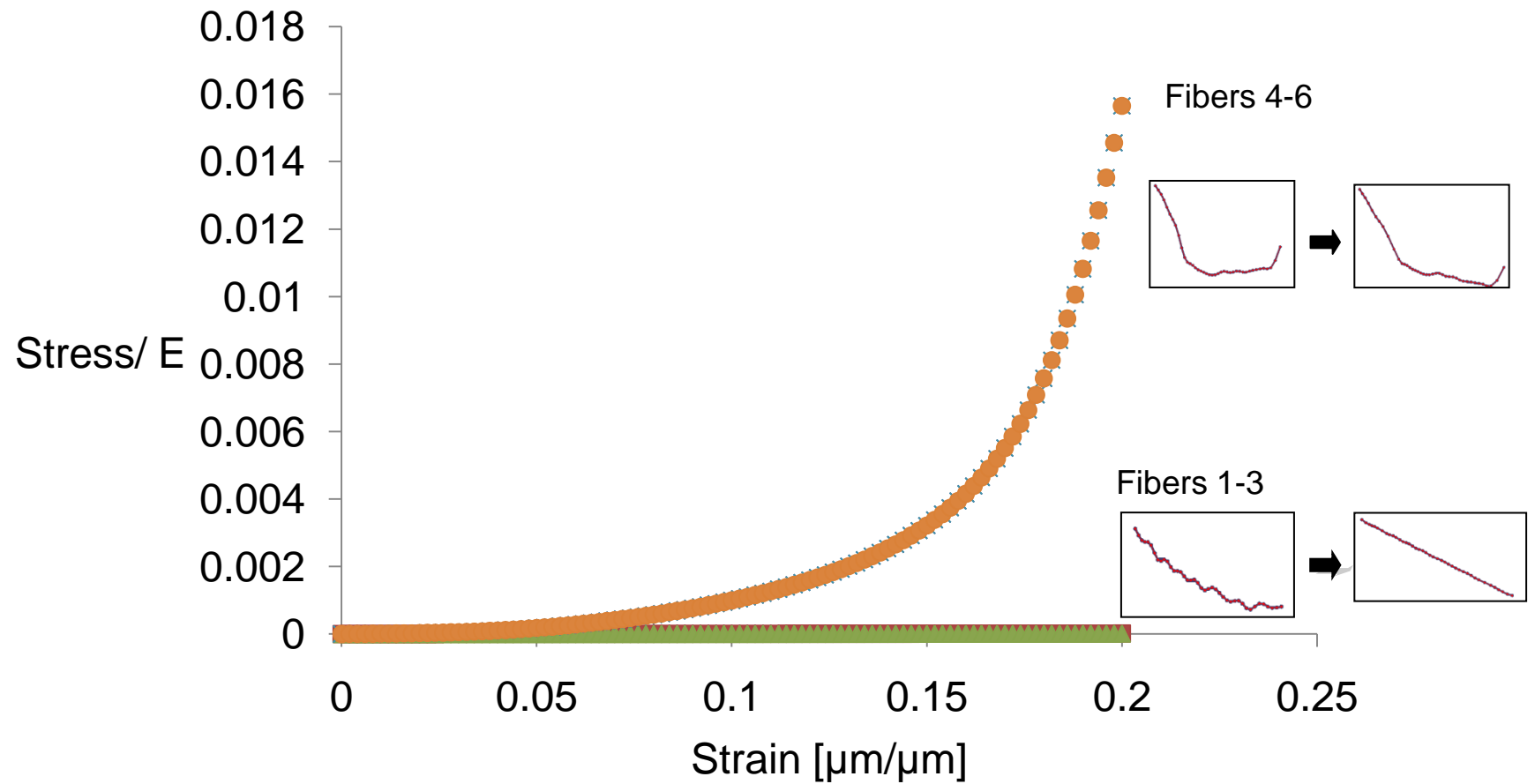


Figure 7: Comparison of normalized stress versus strain of fibers listed in Table 3.

3.2 Geometric changes in single fibers from 0 to 20% strain

3.2.1 Fourier coefficient changes

3.2.1.1 Proportional decrease of Fourier amplitudes

Strained fibers with elastic moduli of 10, 100, and 1000 MPa exhibited a decrease in Fourier amplitudes as compared to initial Fourier amplitudes of the unstrained fibers. This is depicted in Figure 8.

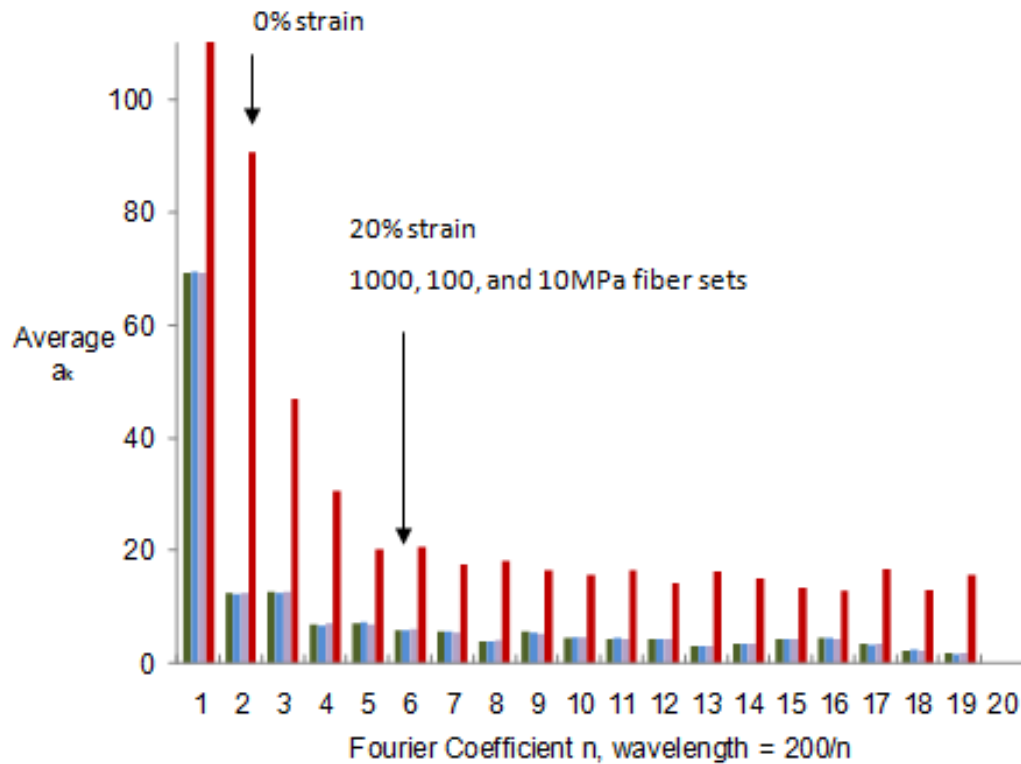


Figure 8: Average amplitudes of Fourier coefficients for fibers in the non strained

The average decrease for fiber amplitudes in all three moduli fiber sets was found to be relatively consistent, at $75\pm 7\%$. Figure 9 reports the average percent change from initial geometry to 20% strained geometry in a graphical manner for each fiber set corresponding to fiber moduli of 10, 100, and 1000 MPa.

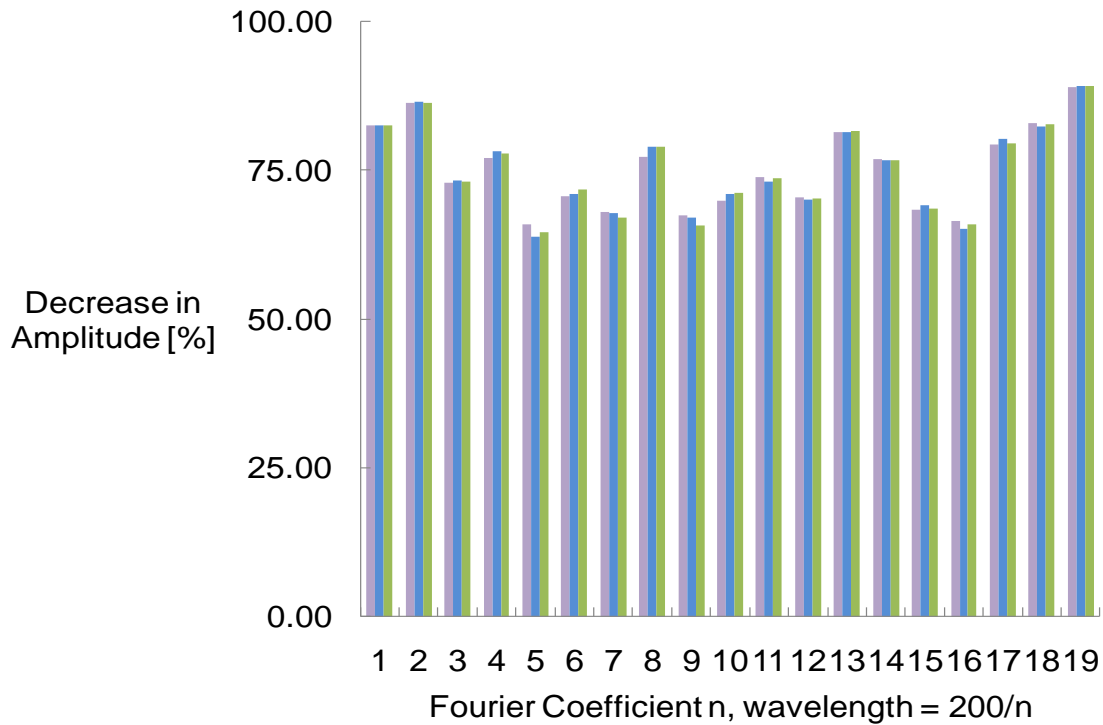


Figure 9: Average percent decrease in amplitude from unstrained to 20% strained geometry for each Fourier coefficient. Data is presented for fibers with E=10MPa (green), E=100MPa (blue), and E=1000MPa (purple)

3.2.1.1 Paired t-test rejection of unique Fourier signatures based on moduli

Fourier coefficients of the 20% strained geometries for each fiber set failed to reject the null hypothesis of a matched pair t-test. Thus, the Fourier coefficients of the 20% strained fibers from the 10, 100, and 1000MPa fiber sets were not determined to belong to separate populations. P-values for each comparison calculated are reported in Table 3.

Table 3: Average amplitudes of Fourier coefficients for fibers in the non strained condition, as well as fibers of 10, 100, and 1000MPa at the 20% condition

Fourier coefficients compared	Paired fiber moduli sets, moduli in Mpa		
	10 and 100	10 and 1000	100 and 1000
n = 1	0.22	0.32	0.32
n = 2	0.43	0.32	0.32
n = 3	0.20	0.32	0.32
n = 4	0.16	0.32	0.32
n = 5	0.17	0.32	0.32
n = 6	0.78	0.32	0.32
n = 7	0.83	0.32	0.32
n = 8	0.33	0.32	0.32
n = 9	0.83	0.32	0.32
n = 10	0.42	0.32	0.33
n = 11	0.22	0.32	0.32
n = 12	0.18	0.32	0.32
n = 13	0.75	0.32	0.32
n = 14	0.56	0.32	0.31
n = 15	0.24	0.32	0.32
n = 16	0.17	0.32	0.32
n = 17	0.24	0.32	0.32
n = 18	0.17	0.32	0.32
n = 19	0.24	0.32	0.25

3.2.2 Tortuosity changes

The average tortuosity of all three fibers sets after 20% strain was 1.03, which exhibits a 12.4% decrease from the initial average tortuosity of the unstrained fibers. Final tortuosity values averaged for each fiber set is depicted in

Figure 10. Matched pair t-tests confirmed independence of fiber moduli on the change in tortuosity of a fiber between 0 and 20% strain. The results of the matched pair t-test can be found in Table 4.

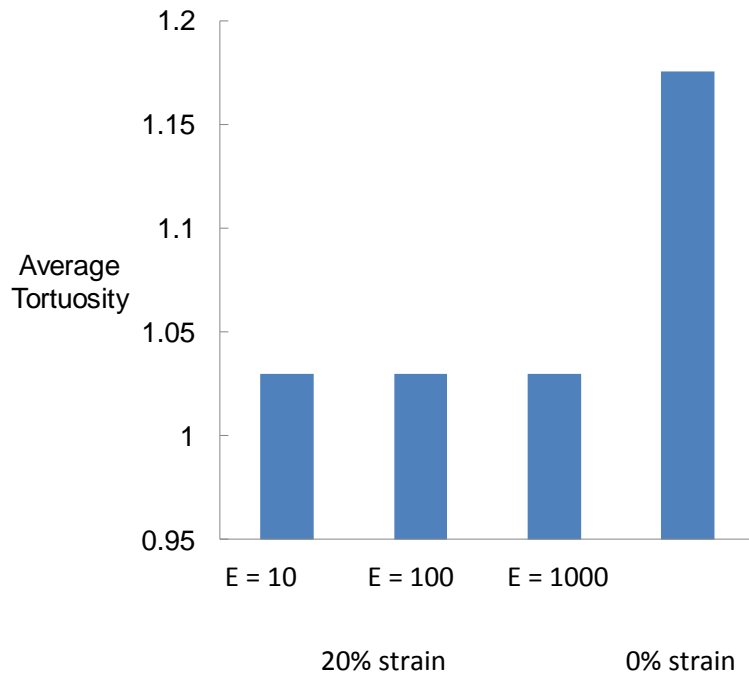


Figure 10: Average amplitudes of Fourier coefficients for fibers in the non strained condition, as well as fibers of 10, 100, and 1000MPa at the 20% condition

Table 4: Matched pair t-test results for the comparison of average tortuosity values in the 20% strain fiber sets

Moduli compared in Mpa	P-value
10 and 100	0.18
10 and 1000	0.32
100 and 1000	0.35

CHAPTER 4: DISCUSSION

This chapter evaluates results of the study first with respect to the stress-strain behavior of single fibers based on initial geometry as well as modulus in section 4.1. Section 4.2 discusses the independence on modulus of single fiber geometry changes with respect to strain, and provides explanations of potential mechanisms which led to the effects observed in this study.

4.1 Stress-strain behavior of single fibers in uniaxial deformation

Fibers in this study exhibited normalized stress-strain behavior (σ/E vs ϵ) that was independent on fiber modulus, yet influenced by the initial and final tortuosities of the fiber.

4.1.1 Tortuosity dependence

As depicted in Figure 7, the degree of tortuosity of a fiber altered the σ/E vs ϵ behavior of a fiber in the 0 to 20% strain regime. More tortuous fibers exhibited more compliance, so that stress increased more gradually with strain as compared to less tortuous fibers. This effect of tortuosity on the stress-strain behavior of can be accounted for by the relationship between fiber tortuosity and the source of fiber stress during straining. The resulting stress in a fiber during a uniaxial pull is the result of two components. The first source component is the stress generated from increasing the bond lengths between the backbones of the polymer chains. The second source component is the stress generated

from decreasing the overall tortuosity of the fiber. The ratio of produced stress to gained strain for the first component is orders of magnitude higher than the second component as the bonds between polymer backbones are very stiff. As a result, when a fiber exhibits high tortuosity, a large percentage of initial strain is due to the component that will yield the most strain for the amount of generated stress, decrease in the overall tortuosity of the fiber, and will thus exhibit a low increase in stress as the fiber extends. When fiber exhibits low tortuosity, however, the component of stress generation driven by increasing bond distances between the polymer backbones dominates as the contributor to stress generation within the fiber and stress rises at an increasing rate as the fiber extends.

4.1.2 Modulus independence

Figure 7 indicates that the normalized stress (σ/E) in a fiber during strain is independent of fiber modulus. This is most likely the result of the relation between the slope of a deflection curve, v , and the elastic moduli in cases of applying a force to an originally straight beam. An example of this relationship for a beam fixed at one end is,

$$v = \frac{Px}{2EI}(2a - x) \quad \text{Equation 4}$$

where x is the distance along the beam in the x direction, I is the moment of inertia of the beam, a is the distance of the fiber section from the point of force application, and P is the force applied to the beam [13].

If the straightening of a bulk material follows this relationship between changes in the slope of the beam, then the stress developed in the fiber will be a function of the E of the fiber. As a result, during the process of normalizing the stress curves by distributing stress over E of the material, the E of a single fiber during strain would be removed as a variable which influences force in a fiber during straining. Thus, the stress-strain behavior of a fiber would be independent of fiber modulus.

4.2 Single fiber geometry changes between strained and unstrained conditions

Fiber geometry changes based on a final strain of 20% in fibers originating from the same geometries, was found to be independent of fiber modulus as reported in Figure 8.

Additionally, average fiber Fourier coefficient amplitudes with respect to 10, 100, and 1000MPa modulus fiber sets were observed to exhibit proportional reduction of Fourier coefficients during extension as reported in Figure 9.

4.2.1 Independence of average geometry changes with respect to fiber elastic modulus

Average change in both Fourier coefficients as well as tortuosity for fibers from all three sets appeared to be independent of fiber modulus as seen in Figure 7. Although nominal disparities can be found between the changes in Fourier coefficients as well as tortuosity value changes before and after 20% strain, matched pair t-tests resulted in the inability to reject the null hypothesis that the fiber sets belong to distributions with different means.

4.2.2 Proportional reduction in Fourier amplitudes during straining

As depicted in Figure 8 and Figure 9, Fourier coefficient amplitudes in all fibers exhibited proportional reduction. The average reduction was 75% with a standard deviation of 7%. Percent reductions of all 19 average Fourier coefficients from 0 to 20% strain geometries for each modulus set, were within two standard deviations. This would seem to indicate that average percent reduction in Fourier amplitudes of single fibers during straining is comparable.

4.2.3 Proposed relationships between individual fiber moduli and fiber geometry changes *in vitro* fiber extension

This study indicated that once fiber geometry is set to an initial shape, stiffness does not affect the resulting shape of the fiber after deformation. This study, however, does not focus on the relationship between fiber modulus and the unstrained shape of the fiber. In order to enable the use of analysis procedures such as matched pair t-tests, initial fiber geometry of each stiffness fiber set was equivalent. As a result, the effect of fiber modulus on initial fiber shape was not explored. In previous studies, the stiffness of a material and the shape of a material have been found to be related as quantified through properties such as persistence length and flexural rigidity. As a result, rather than affecting micro-deformation of a scaffold during strain, it is possible that modulus of a scaffold material affects changes in fiber geometry by affecting the initial configuration of the scaffold before strain as initial configuration of the scaffold. This is potentially supported by the influence of initial configurations such as tortuosity, which were shown to have significant effect on the geometric deformation behavior of a fiber, such as the

Force-strain curves exhibited in Figure 7. Additionally, current work has indicated that fibers fabricated from varying elastic modulus also form distinct geometries [15].

CHAPTER 5: CONCLUSIONS AND FUTURE WORK

5.1 Conclusions

This study determined the following conclusions:

- 1 The normalized stress-strain behavior (σ/E vs ϵ) of single fibers is independent of fiber elastic modulus (E), but it is influenced by fiber tortuosity.
- 2 The evolution of fiber geometry with deformation is independent of fiber modulus.
- 3 As fibers are strained, amplitudes of wavelengths averaged over various initial fiber geometries, appear to reduce proportionally. Specifically this study revealed a $75\pm 7\%$ reduction in wavelength amplitude from 0 to 20% strain.

5.2 Future work

As a final confirmation of proportional decrease in Fourier coefficient amplitudes during deformation, the decrease in Fourier coefficient amplitudes on an individual fiber basis will be analyzed further for statistical trends. This will reduce the possibility of the proportional amplitude decreases of varying wavelengths being a result of the randomness of initial fiber geometries and the large sample size utilized in this study.

Future work also includes further investigation of the relationship between scaffold micro-deformation, cellular changes, and cell signaling. This investigation will further contribute to the characterization of the mechanical stimulation process and will correspond with relationships 2 and 3 depicted in Figure 2.

BIBLIOGRAPHY

1. Ingber DE, Mow VC, Butler D, et al. Tissue engineering and developmental biology: Going biomimetic. *Tissue Engineering* 2006;12(12):3265-3283.
2. Lanza R, Langer R, Vacanti J. Introduction to Tissue Engineering. In: *Principles of Tissue Engineering*. Elsevier science Ltd, Oxford. 2008. pp3-4.
3. Patrick CW, Mikos AG, McIntire LV. Prospects of tissue engineering. In: *Frontiers in Tissue Engineering*. Elsevier Science Ltd, Oxford. 1998. pp. 3-11.
4. www.transplantliving.org. United Network for Organ Sharing. 2011, April 2.
5. optn.transplant.hrsa.gov and OPTN/SRTR Annual Report via www.organdonor.gov. 2001, April 2.
6. Boyce ST, Kagan RJ, Greenhalgh DG, Warner P, Yakuboff KP, Palmieri T, Warden GD. Cultured skin substitutes reduce requirements for harvesting of skin autograft for closure of excised, full-thickness burn. *Journal of Trauma-Injury, Infection and Critical Care* 2006. 60, 821-829.
7. Boyce ST, Kagan RJ, Yakuboff KP, Meyer NA, Reiman MT, Greenhalgh DG, Warden GD. Cultured skin substitutes reduce donor site harvesting for closure of excised, full-thickness burns. *Annals of Surgery* 2002. 235, 269-279.
8. Boyce, S.T., Goretsky, M., Greenhalgh, D.G., Kagan, R.J., Reiman, M.T., Warden, G.D.. Comparative assessment of cultured skin substitutes and native skin autograft for treatment of full-thickness burns. *Annals of Surgery*, 1995; 222(6), 743-752.
9. Nirmalanandham, V.S. Rao, M., Shearn, J.T., Juncosa-Melvin, N., Gooch, C., and Butler, D.L. Effect of scaffold material, construct length and mechanical stimulation on the in vitro stiffness of the engineered tendon construct. *J Biomech*, 2008; 41, 822
10. Mizutani T, Haga H, and K Kawabata. Cellular stiffness response to external deformation: Tensional homeostasis in a single fibroblast. *Cell Motility and the Cytoskeleton* 2004;59(4):242-248.
11. Geraets WG. Comparison of two methods for measuring orientation. *Bone* 1998;23:383-388.

12. Sander EA, Barocas, VH. Comparison of 2D fiber network orientation measurement methods. Wiley InterScience. 19 February 2008 DOI: 10.1002/jbm.a.31847
13. Hibbeler RC. Mechanics of Materials. Prentice Hall. 2007. Ed. 7. Pg. 539.
14. Zwillinger D. CRC Standard Mathematical Tables and Formulae. CRC Press, Boca Raton. 1991.
15. Ebersole GC Anderson PM Powell HM. Epidermal differentiation governs engineered skin biomechanics. J. Biomech. 2010. 43, 3183-90

APPENDIX A

SAMPLE ABAQUS INPUT FILE

```
*NODE
1,      0.000,      100.000,      2.500
2,      5.000,      104.404,      2.500
3,     10.000,      108.812,      2.500
4,     15.000,      115.126,      2.500
5,     20.000,      123.956,      2.500
6,     25.000,      132.281,      2.500
7,     30.000,      138.069,      2.500
8,     35.000,      145.026,      2.500
9,     40.000,      158.146,      2.500
10,     45.000,      175.442,      2.500
11,     50.000,      188.856,      2.500
12,     55.000,      193.811,      2.500
13,     60.000,      193.702,      2.500
14,     65.000,      193.904,      2.500
15,     70.000,      195.340,      2.500
16,     75.000,      195.999,      2.500
17,     80.000,      195.458,      2.500
18,     85.000,      194.918,      2.500
19,     90.000,      194.588,      2.500
20,     95.000,      193.596,      2.500
21,    100.000,      191.535,      2.500
22,    105.000,      188.350,      2.500
23,    110.000,      183.829,      2.500
24,    115.000,      178.710,      2.500
25,    120.000,      174.955,      2.500
26,    125.000,      173.244,      2.500
27,    130.000,      171.562,      2.500
28,    135.000,      168.093,      2.500
29,    140.000,      164.079,      2.500
30,    145.000,      161.672,      2.500
31,    150.000,      160.291,      2.500
32,    155.000,      157.694,      2.500
33,    160.000,      153.645,      2.500
34,    165.000,      149.723,      2.500
35,    170.000,      146.251,      2.500
36,    175.000,      142.509,      2.500
37,    180.000,      139.291,      2.500
38,    185.000,      137.351,      2.500
39,    190.000,      133.139,      2.500
40,    195.000,      120.725,      2.500
41,    200.000,      100.000,      2.500
*NSET,NSET=FIBER1,GENERATE
1, 41
```

```

** element no., node1, node2
*ELEMENT,TYPE=B31
1, 1, 2
2, 2, 3
3, 3, 4
4, 4, 5
5, 5, 6
6, 6, 7
7, 7, 8
8, 8, 9
9, 9, 10
10, 10, 11
11, 11, 12
12, 12, 13
13, 13, 14
14, 14, 15
15, 15, 16
16, 16, 17
17, 17, 18
18, 18, 19
19, 19, 20
20, 20, 21
21, 21, 22
22, 22, 23
23, 23, 24
24, 24, 25
25, 25, 26
26, 26, 27
27, 27, 28
28, 28, 29
29, 29, 30
30, 30, 31
31, 31, 32
32, 32, 33
33, 33, 34
34, 34, 35
35, 35, 36
36, 36, 37
37, 37, 38
38, 38, 39
39, 39, 40
40, 40, 41
*elset,ELSET=FIBER1,GENERATE
1, 40
*elset,ELSET=ALLFIBERS,GENERATE
1,40
*BEAM SECTION,SECT=CIRC,ELSET=ALLFIBERS,MATERIAL=ELASTICFIBER
.5
*MATERIAL,NAME=ELASTICFIBER

```



```

*ELASTIC
100, 0
*NSET,NSET=XMAXNODES
  41
*STEP,NLGEOM,INC=20000
*STATIC
0.01,1.,1e-15,.01
*BOUNDARY
  1,      1,      1,      0.000
 41,      1,      1,     40.000
  1,      2,      2,      0.000
 41,      2,      2,      0.000
  1,      3,      3,      0.000
 41,      3,      3,      0.000
  1,      4,      6,      0.000
 41,      4,      6,      0.000
*EL FILE,FREQ=1
S,
E,
*NODE FILE,FREQ=1
U,
RF,
COORD
*Output, field,frequency=1
*ELEMENT OUTPUT
S,
E,
*NODE OUTPUT
U,
RF,
COORD
*END STEP

```

APPENDIX B

FIBER PREPARATION FOR FOURIER TRANSFORM ANALYSIS CODE

```
%calculate fourier coefficients
%open final file
fid = fopen('E1000coefficients', 'w');
fid2=fopen('E1000coefficientsFFT','w');

%open data file
for loop_ctr = 1:100
    DELIMITER = ',';
    HEADERLINES = 19;
    % Import the file
    newData1 = importdata(sprintf('c%d.dat',loop_ctr),DELIMITER, HEADERLINES);

    % Create new variables in the base workspace from those fields.
    vars = fieldnames(newData1);
    for i = 1:length(vars)
        assignin('base', vars{i}, newData1.(vars{i}));
    end

    %create separate x,y subarrays
    x = data(1:41,2:2)
    y = data(1:41,3:3)
    y = y - 100
    xarray_ctr=1

    %determine y interpolation
    for n=1:41
        if x(n) > (10*xarray_ctr)
            xarray(xarray_ctr)= n
            xarray_ctr = xarray_ctr + 1
        end
    end
    for p=1:21
        ind=xarray(p)
        yh = y(ind)
        yl = y(ind-1)
        xh = x(ind)
        xl = x(ind-1)
        numb = p * 10
        deltay = yh-yl
        deltax = xh-xl
        x_interpolated(p)=(p*10)
```

```

y_interpolated(p)= yh - ( (yh-yl)*(xh-numb)/(xh-xl))
end
y_final(1)=y(1)
% determine y values from 0 to 0
for n=1:20
    arctangent = atan(y_interpolated(20)/(200))
    xcoordinate= (n)*10
    y_interpolated(n)
    % if y_interpolated(1)< y_interpolated(21)
    y_final(n+1)=y_interpolated(n)- xcoordinate* arctangent
end
fprintf(fid,'***%d***\n',loop_ctr)
for p = 1:21
    fprintf(fid,'%12.3d\n',y_final(p))
end
fprintf(fid,'\n')
hold on
plot(x_interpolated,y_interpolated)
%fft stuff
fourier=fft(y)
fprintf(fid2,'***%d',loop_ctr)
for ctr = 1: length(fourier)
    fprintf(fid2,'%d\n',fourier(ctr))
end

end
fclose(fid)
fclose(fid2)

```